JOURNAL OF Materials CHEMISTRY

Ageing of oilfield cement at high humidity: a combined FEG-ESEM and Raman microscopic investigation

C.-S. Deng,[a] C. Breen,[a] J. Yarwood,[a] S. Habesch,[a] J. Phipps,[b] B. Craster[b] and G. Maitland[b]

[a]*Materials Research Institute, Sheffield Hallam University, Howard Street, Sheffield, UK S1 1WB*
[b]*Schlumberger Cambridge Research, High Cross, Madingley, Cambridge, UK CB3 0EL*

Received 28th March 2002, Accepted 23rd July 2002
First published as an Advance Article on the web 20th August 2002

The ageing of oil-well cement, Dyckerhoff class G, under saturated water vapour in the presence of carbon dioxide has been studied using the complementary techniques of Raman microscopy and environmental scanning electron microscopy. This combination of techniques has enabled the key components involved in the surface hydration processes to be identified *in situ*, their time evolution to be monitored directly (without the need for quenching and sample extraction) and this evolution of chemistry/mineralogy to be related to local structural changes. It has also enabled local chemical changes in this highly heterogeneous material to be related to the original cement grain mineralogy. High aspect ratio structural features, rich in aluminium and sulfur, were formed on the grain surface during the ageing process. These were identified as ettringite, which exhibited a diagnostic band at 988 cm^{-1} in the Raman spectrum.

Introduction

Storage and transport of oilfield cements are of critical importance in maintaining their quality and hydration performance. The atmosphere, particularly the humidity to which the cement is exposed during storage and transport, plays a key role in this process. With the combined exposure to water and carbon dioxide, the ageing processes at the surface may be different from the hydration processes occurring in bulk. The resulting chemical changes are particularly crucial for oilfield (class G), as distinct from construction (class A), cement materials. Premature or prolonged setting of oilfield cements can have catastrophic operational consequences. Consequently, additives are used to inhibit the cement hydration to give a crucial time window for placing a mobile cement slurry in its correct position (along an oil well that can be several kilometres long) before it hydrates and sets to form a solid seal. Therefore, small changes in surface hydration/chemistry can cause large variations in the induction or retardation time. Hence, good control and characterisation of cement ageing processes is crucial for process reliability.

The hydration of bulk Portland cements has been extensively studied and sampling is one of the main issues associated with the study of cement hydration.[1] The initial stages of cement hydration, involving various coupled processes, such as dissolution of components, liquid phase transport and surface hydration reactions, still remain unclear. Attempts have been made to study rapid hydration by methods including *in situ* X-ray diffraction of cement slurry under agitation,[2,3] or quenching the hydration reaction by extracting aliquots at selected times during agitation followed by drying.[4] The latter approach requires rigorous de-hydration procedures, and inevitably creates doubt regarding how well the dried sample represents the components of the matrix immediately prior to its removal. Moreover, many of the studies have focused on the "bulk" properties of the cements, whereas the early stages of hydration are more likely to occur on the surface of the cement particles and in the near-surface liquid.[5]

The hydration of pure C_3A has been studied previously,[6] and this was recently revisited and extended to include pure C_3S and C_2S at reduced relative humidities[7] (the nomenclature used here for cement is, C = CaO, S = SiO_2, H = OH, $\bar{S}$ = SO_4, A = Al_2O_3, F = Fe_2O_3). The latter study established that C_3A can hydrate at lower relative humidities than either C_3S or C_2S, and that an induction period was always needed. The presence of carbon dioxide in the water vapour was not considered, and the interaction of the pure phases with minor cement components, such as gypsum, was precluded through the use of pure phases in isolation. Electron microscopic studies of the prehydration of Portland cements using water vapour at 25 and 120 °C did not identify the presence of ettringite.[8,9]

There have been some studies on cement surfaces and surface processes using vibrational spectroscopy. Fletcher and Coveney[10] and Hughes *et al.*[11] used attenuated total reflection Fourier transform infrared spectroscopy (ATR-FTIR) to study the hydration of cement and were able to follow the key processes in the cement hydration. Although ATR-FTIR looks at the surface layer (a few micron thick) of the materials, this method still applies principally to "bulk" processes, since it indiscriminately looks at the particular assembly of components (a broad area of surface materials) that are in the evanescent wave field. The aim of this work is to bring together techniques which can characterise both local chemical and structural changes in an ageing cement material. This requires methods capable of making both types of measurement on lengthscales typical of cement grains (1–100 μm), *in situ* and in real time, in a cement powder/paste without the need to quench and extract samples for remote analysis. The techniques chosen are Raman microscopy (RM) and environmental scanning electron microscopy (ESEM). Raman microscopy enables spectra to be acquired from surface sample zones down to a few microns, with minimal interference from a water environment. On such lengthscales the interference from fluorescence, so often a problem for bulk cement slurries, is also minimised. This technique, therefore, enables spectra characterising the evolving hydration processes to be obtained for individual cement particles. Given the high degree of phase heterogeneity in cement powders, this opens up, for the first time, the possibility of tracking the hydration rates and products of different cement phases (sometimes almost pure, sometimes mixed within a particle or a group of particles) within a real cement environment. Sample acquisition times of less than

1 min allow information to be obtained at very early times in the hydration process. Access to this crucial, early phase of the process, during which much of the controlling surface coating processes by early reaction products are determined, cannot be readily obtained by other techniques.

ESEM operates under a low water vapour pressure and is an ideal technique for studying the effects of a controlled humidity environment. It enables the structural changes accompanying cement hydration to be mapped at the micron level and, through EDX analysis, gives complementary information on local chemical composition. Ideally, Raman and ESEM analysis would be carried out simultaneously and continuously in the same instrument, but such a device does not yet exist. The current study demonstrates the benefits of combining these techniques to study the atmospheric ageing problem and the potential of a future combined instrument for a fuller *in situ* investigation of cement hydration.

Bensted,[12] in his pioneering work, collected Raman spectra from the individual mineral components in cements and of the hydration products, including ettringite $\{Ca_6[Al_2(OH)_{12}]\cdot(SO_4)_3\cdot 26H_2O\}$. Raman spectroscopy is also a powerful technique for detecting carbonate through the v_1 $[CO_3^{2-}]$ band due to its high scattering cross-section.[13,14] Dyer *et al.*[15] also collected Raman spectra for pure cement minerals. Tarrida *et al.*[16] were able to follow the hydration process of alite (C_3S) with Raman spectroscopy; they observed the formation of the gel phase C–S–H and CH as C_3S was hydrated and derived the kinetics of the hydration. Kirkpatrick *et al.*[17] used their earlier nuclear magnetic resonance work[18] to help make Raman assignments for synthesised C–S–H gel, and for tobermorite and jennite, which are closely related structurally to the gel. These reports have underpinned our study of oilfield cement under high humidity.

There have been numerous reports on cement hydration using scanning electron microscopy, either for pure component minerals[19] or Portland cements.[20] There have been many fewer studies using ESEM on cement hydration since Meredith *et al.*[5] first observed the morphological evolution during C_3S hydration *in situ*. In combination with conduction calorimetry, they observed the different stages of morphological change. The initial stage was the formation of an amorphous gel layer, $\sim$20–30 nm thick, around the C_3S particles as water was brought into contact with the particles. This was followed by a dormant period, ending with formation of more crystalline materials in the layer. More recently, Stark *et al.*[21,22] used ESEM to study the hydration of some Portland cements, as well as C_3S, C_2S, C_3A and C_4AF. Their results suggested that similar stepwise processes occurred in the hydration of Portland cements, and they observed that ettringite was the first product to appear, only 10 min after water was introduced. None of these studies provided chemical change data along with the morphological evolution, perhaps due to the short times involved in the initial stages of hydration.

In this present study, Raman microscopy, has been used to study the surface hydration of the cement powder as a whole and of individual particles within the cement powders. These contain the key components that initiate and/or control the hydration process. In addition, ESEM has provided images of cement surfaces in the absence of an applied conductive layer, thus allowing direct observation of the sample morphology at higher resolution. Energy-dispersive X-ray spectroscopy (EDX) analysis provides complementary elemental information which helps to identify the individual phases.

Materials and experimental

A Dyckerhoff class G oil-well cement was used for the study. Its chemical composition, derived from X-ray fluorescence (XRF) analysis, is presented in Table 1 and the derived Bogue phase composition in Table 2, according to the procedure detailed by Taylor.[23] The phase composition derived using modified Bogue calculation suggests no C_3A in the cement (Table 2), in agreement with XRD results for the cement powder. The total oxide content was 97.1%, which reflects the loss of water and other volatile components at high temperature during bead preparation prior to analysis. The individual cement mineral components were purchased from CTL (USA) and used without further treatment.

Table 1 Oxide content of Dyckerhoff class G cements by XRF

Oxide	Content/mass%	Oxide	Content/mass%
Na_2O	0.16	TiO_2	0.18
MgO	0.73	Mn_3O_4	0.17
Al_2O_3	3.86	Fe_2O_3	4.64
SiO_2	22.52	ZnO	0.01
P_2O_5	0.05	SrO	0.16
SO_3	0.37	ZrO_2	<0.01
K_2O	0.71	BaO	0.03
CaO	63.53	HfO_2	<0.01

Sum = 97.11

Table 2 Bogue phase composition derived from XRF data

Phase	Composition/mass%
Alite	60.5
Belite	21.4
Aluminate	0
Ferrite	19.1

The cement powder was loaded into a plastic container ($\sim$1 cm in diameter and 1 cm deep) and the surface flattened by pressing lightly with a microscope slide. For the water vapour hydration studies, the sample was placed in a sealed desiccator, the lower part of which was filled with distilled water, and kept at ambient temperature. The sample was removed at preselected time intervals and Raman spectra recorded at selected positions. These spectra were acquired using a Renishaw System 2000 Raman spectrometer which comprised an integral Raman microscope (Olympus BH2 system), a stigmatic single spectrograph and a Peltier-cooled CCD detector (400 $\times$ 600 pixels). The holographic notch filters allowed a lower spectral limit of $\sim$150 cm^{-1}. The excitation source used was a 632.8 nm (25 mW) He–Ne laser. A maximum throughput of 4–5 mW was possible at the sample down to a 2 μm spot *via* a standard 50$\times$ microscope objective. The Raman shift was calibrated before each experiment using the 520 cm^{-1} peak of silicon at a magnification of 50$\times$. Spectra recorded on samples after such calibration at different times and with different objectives indicated an error of $\pm$0.5 cm^{-1} in the Raman shift. The spectra were recorded by selectively focusing on the sample surface. Objectives of 5$\times$ to 50$\times$, which correspond to sample areas of *ca.* 30 to 2 μm diameter, respectively, were used. Normally, a 5 $\times$ 10 s collection time was used for each spectrum. Laser induced heating was not an issue, since repeat spectra showed no differences. The detailed sampling method involved: (i) recording a spectrum using the lowest magnification objective (5$\times$), then (ii) recording spectra with objectives of greater magnifications (20$\times$ and, finally, 50$\times$) whilst the sample was kept in position. At higher magnification, it was necessary to refocus the sample. Generally, up to 10 spectra were recorded at randomly selected points on the sample, choosing particles having different colours, in rough proportion to the phase composition [*i.e.* 7 white particles (silicates) plus 3 dark particles (aluminoferrite), at different positions] so as to be as representative as possible. It is accepted that as a result of the heterogeneity in the samples within the area

the Raman laser probes, such a sampling method may not include all the features on a surface, but repeated observations confirmed that it was sufficient to be representative. Bands due to several phases may exist in one spectrum. However, it is stressed that the characteristic/strongest bands for different phases are distinctly resolvable. For example, as illustrated later, the v_1 (SiO_4^{4-}) bands for Si–O vibrations in alite and belite appear at $\sim$830–850 cm^{-1}, the band maxima appear at different wavenumbers, $\sim$835 cm^{-1} for alite and $\sim$850 cm^{-1} for belite. The new phases formed exhibited their own characteristic bands, different from those in the raw cement. Therefore, although this sampling method may not report all the chemical changes in the materials, all the bands are assigned and are considered to be representative of the principal structural changes occurring at the surface as the ageing progresses.

ESEM images were obtained using a Philips FEI XL30 ESEM-FEG, equipped with an Oxford Instruments ISIS/300 light element detector (Pentafet) using water vapour as the ionising gas. The water vapour pressure was kept as low as possible, typically at 2 torr, when recording EDX mapping for the sample, to reduce the interference of the ionised species on the X-ray signal. To achieve good contrast during imaging, a water vapour pressure $\geqslant$5 torr was normally used. An accelerating voltage of 20 kV, at a working distance of 10 mm, and a beam current of 2 nA were employed. For quantitative analysis, a standardless approach and a ZAF correction were used. A take-off angle of 35° with a flat specimen was used. During analysis, the temperature in the chamber was 18–20 °C, with relative humidity up to 60%.

Results and discussion

1 Raw cements

Fig. 1 presents a typical ESEM image of a cement powder, which shows it contained particles of sizes from *ca.* 50 to $<$1 μm with irregular morphology. EDX spectra of randomly selected particles confirmed the presence of the oxides listed in Table 1.

The main silicate phases of Dyckerdoff class G cement powders (C_3S, C_2S) and C_3A (see Table 2 for an analysis derived from Table 1 based on the procedure of Bogue) are all lightly coloured, or white, whereas the ferrite is known to be dark brown or black under an optical microscope. Gypsum particles are also white. The Raman spectra of the standard phases (Fig. 2) were used to identify the components interrogated by the Raman technique in the cement powders. The crystal structure of standard C_3S (alite) was monoclinic, as in the cement, C_2S (belite) was monoclinic stabilised with Al_2O_3–MgO (β-C_2S), but the amount of Al_2O_3 and MgO is unknown. C_3A (aluminate) was cubic. The assignments of the bands observed in pure component minerals along with those for other materials are summarised in Table 3.[12,16,17,24–26] The ettringite sample [Fig. 2(B), spectrum (ii)] contained a small amount of carbonate (v_1 [CO_3^{2-}] at 1086 cm^{-1}).

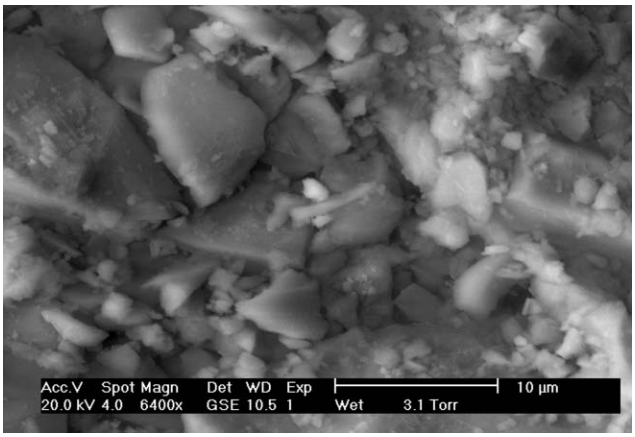

Fig. 1 An ESEM image of raw Dycherhoff class G cement powder.

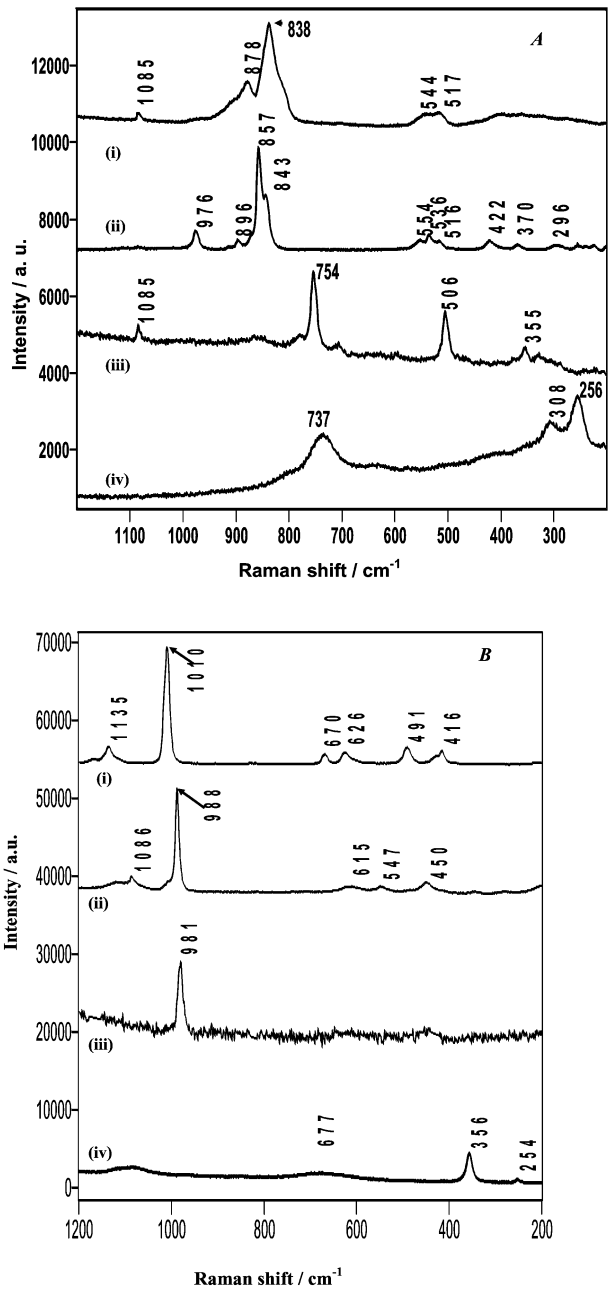

Fig. 2 Raman spectra for standard cement minerals. (A) (i) C_3S (monoclinic), (ii) C_2S, (iii) C_3A and (iv) C_4AF; (B) (i) gypsum, (ii) synthetic ettringite, (iii) concentrated aqueous (0.5 M) SO_4^{2-} solution and (iv) solid $Ca(OH)_2$.

Measurements recorded under higher magnification, particularly 50×, resulted in significantly different spectra at different positions (Fig. 3), due to the heterogeneity in the materials at this reduced sampling area. These represent the range of spectra obtained from the cement powders. Each individual spectrum exhibited the characteristic strong bands for particular minerals, although the bands often overlapped. For example, in spectrum (i) in Fig. 3, the strongest band is at 827 cm^{-1}, assigned to the Si–O stretching mode in alite.[17] Fig. 3(ii) is a spectrum of predominantly belite, with the strongest band at 857 cm^{-1}. In addition to these Si–O bands, there are broad bands of medium intensity at $\sim$715 cm^{-1}, suggesting the incorporation of Fe^{3+} in the alite or belite

Table 3 Assignment of principal Raman bands for cement minerals

Material	Raman shift/cm^{-1}	Assignment	Material	Raman shift/cm^{-1}	Assignment
C_3S (monoclinic)	838, (s)	ν_1 [SiO_4^{4-}]	Carbonate (calcite)	1087 (s)	ν_1 [CO_3^{2-}]
	544, 517 (w–m)	ν_4 [SiO_4^{4-}]		879 (m)	ν_2 [CO_3^{2-}]
				714 (m)	ν_4 [CO_3^{2-}]
				280 (m)	($\nu_3 - \nu_1$) [CO_3^{2-}]
C_2S	857 (s)	ν_1 [SiO_4^{4-}]	Gypsum	1010 (s)	ν_1 [SO_4^{2-}] (position varies greatly in solid)
	976 (w)	ν_3 [SiO_4^{4-}]		491 (w–m)	ν_2 [SO_4^{2-}]
	554, 536, 516 (w–m)	ν_4 [SiO_4^{4-}]		1135 (w–m)	ν_3 [SO_4^{2-}], may split to 2 or 3 bands
	422 (w–m)	ν_2 [SiO_4^{4-}]		626 (w–m)	ν_4 [SO_4^{2-}], may split to 2 or 3 bands
C_3A	754 (m)	ν_3 [AlO_4^{5-}]	Ettringite	988 (s)	ν_1 [SO_4^{2-}]
	506 (w–m)	ν_1 [AlO_4^{5-}]		615 (w–m)	ν_4 [SO_4^{2-}], may split to 2 or 3 bands
				450 (w–m)	ν_2 [SO_4^{2-}]
C_4AF	737 (m)	ν_1 [(Fe, Al)O_4^{5-}], or [(Fe, Al)O_6^{9-}]	C–S–H gel	850 (w–m)	Si–O–Si stretch
	308 (w–m)	ν_4 [(Fe, Al)O_4^{5-}], or [(Fe, Al)O_6^{9-}]		680, 620 (w)	Si–O–Si bending
	256 (m)	ν_2 [(Fe, Al)O_4^{5-}], or [(Fe, Al)O_6^{9-}]		450 (w)	Internal deformations of $[SiO_4]^{4-}$ tetrahedra
CH	677 (w)	ν_3 $Ca(OH)_2$			
	356 (s)	ν_2 $Ca(OH)_2$			
	254 (w–m)	ν_4 $Ca(OH)_2$			

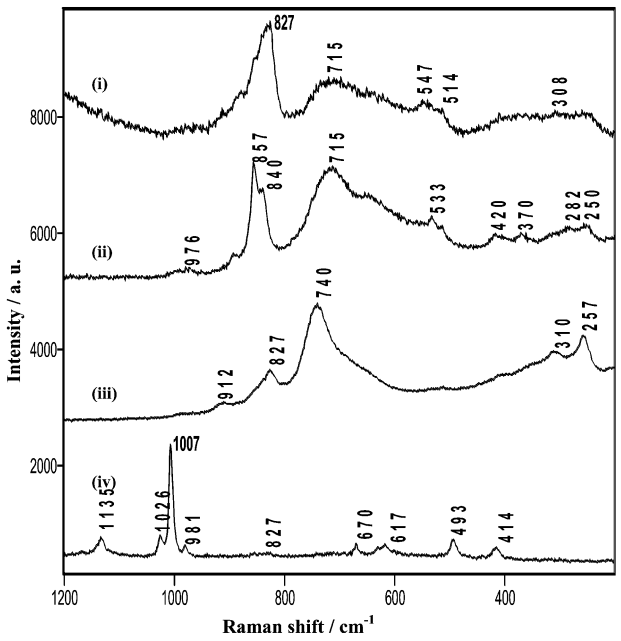

Fig. 3 Raman spectra for Dycherhoff class G cement, recorded using a 50× objective: (i) and (ii) were recorded on white particles, (iii) was recorded on a dark particle. The spectra revealed heterogeneity in the materials, *i.e.* (i) and (ii) are predominantly alite (C_3S) and belite (C_2S), respectively, but also with bands associated with aluminoferrite (C_4AF); (iv) is a spectrum for gypsum particles in the cement.

structure.[24] This region also contains the characteristic vibrations of aluminoferrite (C_4AF), as shown clearly in Fig. 3(iii), which has a strong band at 740 cm^{-1} and weaker bands at 310 and 257 cm^{-1}. The broad band in the 700–750 cm^{-1} region perhaps reflects the fact that C_4AF can encompass a range of solid solutions of various Ca–Al–Fe–O content. The presence of amorphous materials derived from these structures or their hydration products is also possible.[27] The strong bands at 1007 cm^{-1}, together with those of low intensity at 670, 617, 493 and 414 cm^{-1} [Fig. 3(iv)], are typical for gypsum particles in the cement.

The overall features in these spectra also suggest that the particles were intimately mixed down to the scale of a few microns sampled by the laser spot, indicating a high degree of local heterogeneity. It has been reported that individual cement particles can be solid solutions of different phases, and that interstitial phases exist in the main phases.[28]

2 After exposure to water vapour

2.1 Raman spectroscopy. The Raman spectra taken on white particles (within the class G powder) after 1 week, 1 month and 3 months' exposure to water vapour (Fig. 4–6) show that some reactions have occurred. After 1 week, bands assigned to Portlandite at 670, 357 and 255 cm^{-1} appeared

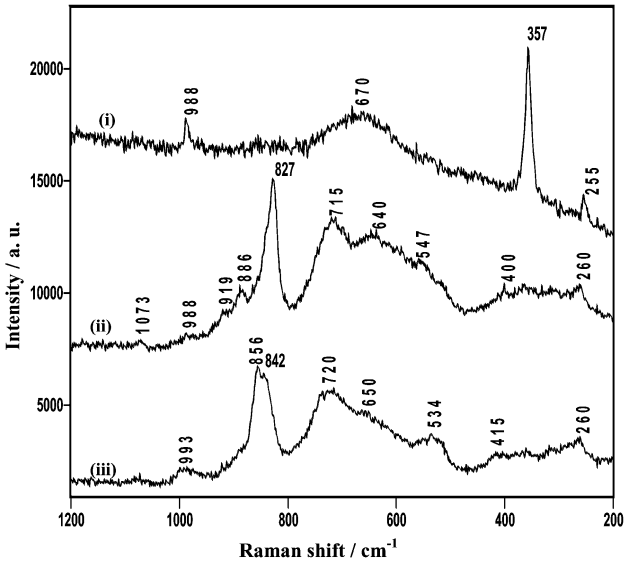

Fig. 4 Raman spectra recorded on white particles (at different positions on the sample) after 1 week's exposure to water vapour using a 50× objective.

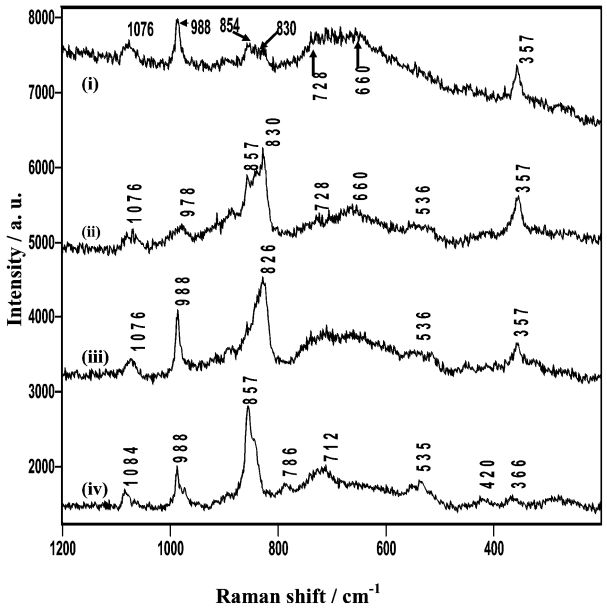

Fig. 5 Raman spectra recorded on white particles (at different positions on the sample) after 1 month's exposure to water vapour using a 50× objective.

[Fig. 4(i)]. A band at 988 cm^{-1}, assigned to the v_1 [SO_4^{2-}] of ettringite, was also present. The ettringite crystals could not be seen with an optical microscope, but ESEM micrographs (*vide infra*) confirmed that the high aspect ratio features associated with ettringite[21,22] did appear after 1 week's exposure to water vapour. The trace also exhibited a broad band centred around 670 cm^{-1}, which is similar to that at 677 cm^{-1} in the spectrum of $Ca(OH)_2$ [Fig. 2(B), spectrum (iv)], although others have assigned a band at 660 cm^{-1} to C–S–H gel in sulfate-free systems.[13] However, the combination of the broad band at 670 cm^{-1}, together with the strong, sharp band at 357 cm^{-1}, indicated the presence of Portlandite. This species was not observed at all locations, particularly where alite [Fig. 4(ii)] and belite [Fig. 4(iii)] exhibited strong signals. There were traces of Portlandite in the spectra obtained after 1 month's exposure (Fig. 5), which was probably due to the hydration of the silicates. Furthermore, the band at 988 cm^{-1} (v_1 [SO_4^{2-}]) became prominent and was present at each position measured on the sample, suggesting that mass transfer involving sulfate resulted in the formation of ettringite. Rudimentary fitting of the band at 988 cm^{-1} in Fig. 5(iv) identified that there was a shoulder at 976 cm^{-1}, which was assigned to v_3 [SiO_4^{4-}] of belite [Fig. 2(A), spectrum (ii)]. The band at 830 cm^{-1} associated with alite was still strong in some locations after 1 month. However, after 3 months' [Fig. 6(A) and (B)], the spectra recorded with 5× objective [Fig. 6(A)] showed that the relative intensity in the ~830 cm^{-1} region had diminished significantly. Indeed the spectra recorded at higher magnifications [Fig. 6(B)] revealed that the band in this region for Si–O stretching was now characteristic of belite, at ~857 cm^{-1}. This was a general trend, although it must be noted that the bands for Si–O in alite were also occasionally observed near 830 cm^{-1}. These results suggest that the early stage of hydration occurred chiefly on alite (C_3S), in agreement with the observations on the hydration of cement with liquid water,[1] causing this to be depleted more rapidly than the less reactive belite (C_2S). Finally, the bands at 1083, 710 and 275 cm^{-1}, assigned to carbonate, also increased with extended exposure at the expense of the 357 cm^{-1} Portlandite band.

The spectra recorded on the dark particles (not shown here) suggested that the reaction involving C_4AF was less clear. The band at ~740 cm^{-1} associated with C_4AF remained

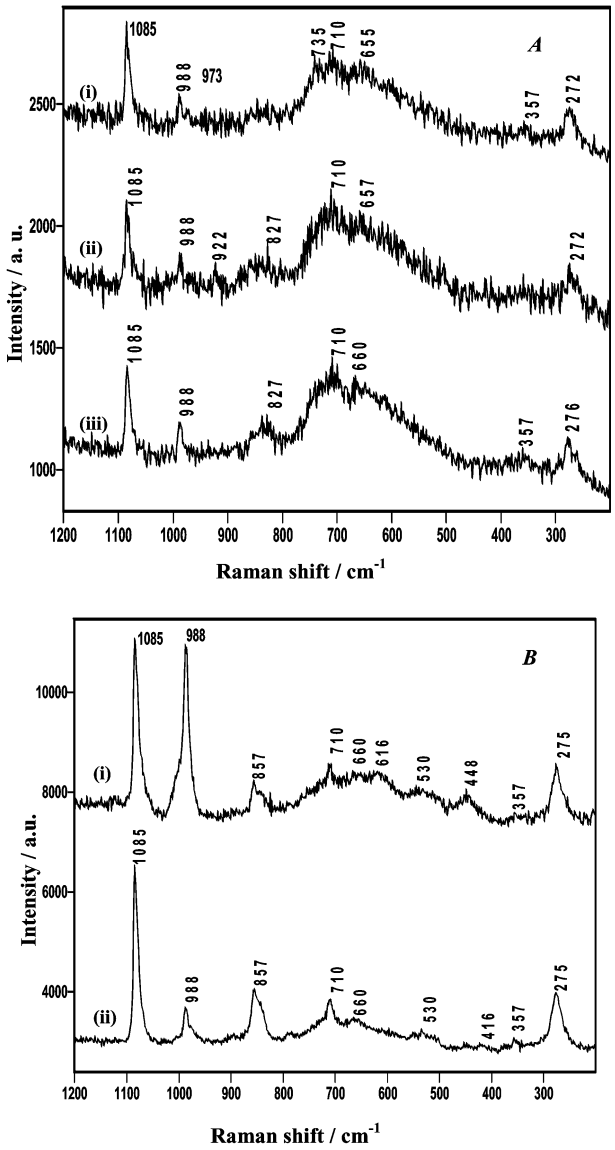

Fig. 6 Raman spectra of white particles after 3 months' exposure to water vapour, recorded with different objectives: (A) 5× and (B) 50×. Spectra were recorded on white particles at different positions with each objective.

strong throughout. It is noted that the 988 cm^{-1} band associated with the sulfate group was present after 1 month, but was weaker after 3 months. This was perhaps a reflection of mass transfer of the sulfate, in that the sulfate dissolved in condensed surface water, thus facilitating a more widespread distribution of such species. This also suggests that a continuous liquid layer existed on the cement surface, which played a crucial role in the ageing process of the cement. It not only provided the liquid phase that hydrated the silicates, but also allowed for the mass transfer of materials, such as the dissolution of carbon dioxide, which accelerated the carbonation of the Portlandite, thus accelerating the further ageing of cement minerals. It was observed that the intensity of the 988 cm^{-1} (ettringite) band recorded on dark particles was much weaker than that on white particles in the class G powder.

In the absence of a sharp, strong v_4 band for $Ca(OH)_2$ at 257 cm^{-1}, the intensity in the 620–680 cm^{-1} region after 3 months' exposure to water vapour (Fig. 6) must be attributed to the formation of C–S–H gel.[16,17] Moreover, the much reduced intensity in the v_1(SiO_4^{4-}) region where alite and belite scatter supports this interpretation. The width of this feature probably reflects the largely amorphous nature of the C–S–H gel. Kirkpatrick *et al.*,[17] in their study of synthesised C–S–H

gel, observed bands at ~980–1010 cm^{-1}, which they assigned to Si–O stretch in C–S–H gel. In our study, bands in this region associated solely with Si–O have not been observed. The reason for this difference is currently unresolved, but may be attributed to a difference in the structure of the materials studied, in that their C–S–H gel may have been more crystalline than that produced herein. However, the initial spectra (Fig. 3) for the raw powders also exhibited quite strong intensity in this region. The strong scattering from interstitial phases, C_3A and C_4AF, and, particularly, the hydration product, Portlandite (675 cm^{-1}), may also have obscured the bands for C–S–H gel.

Special attention was paid to the identification of the high aspect ratio, needle-like features which grew on the cement. The Raman spectra encompassing the fibrous structures observed in ESEM (*vide infra*) as presented in Fig. 6(B), spectrum (i), (after 3 months' exposure to water vapour) should be compared with those for synthetic ettringite and other sulfates that might be present [Fig. 2(B)]. A prominent band appeared in the hydrated sample spectrum at ~988 cm^{-1}. The bands in this region may have complicated origins, including sulfate, such as gypsum, solid aluminium sulfate and other sulfates in the raw cement powders, sulfate ions [from dissolved $CaSO_4$, or $Al_2(SO_4)_3$ in hydrating water], or ettringite. Fig. 2(B) indicates that, although the difference may be small in some cases, the principal peak, ν_1 [SO_4^{2-}] for the different forms of sulfate, appeared at readily distinguishable Raman shifts. Furthermore, comparison of the Raman band positions in the low wavenumber regions of the spectra in Fig. 6(B), spectrum (i), (616, 448 cm^{-1}) with those for synthetic ettringite in Fig. 2(B) (615, 450 cm^{-1}) suggest unambiguously that this 988 cm^{-1} band is due to the sulfate in ettringite. X-Ray diffraction studies also supported the presence of ettringite. The bands at 1085, 710 and 276 cm^{-1} in Fig. 6(B), spectrum (i), are due to carbonate, which can coexist with ettringite in one of three ways. Firstly, calcite ($CaCO_3$, ν_1 [CO_3^{2-}] = 1086 cm^{-1}), formed from the carbonation of Portlandite [$Ca(OH)_2$], may coexist with ettringite in a simple physical mixture. Secondly, the calcium carbonate may be a direct product of the decomposition of ettringite by atmospheric CO_2, according to eqn. 1.

$$3CaO{\cdot}Al_2O_3{\cdot}3CaSO_4{\cdot}32H_2O + 3CO_2 \rightarrow 3CaCO_3 + CaSO_4{\cdot}2H_2O + Al_2O_3{\cdot}xH_2O + (26 - x)H_2O \quad (1)$$

The decomposition products $CaCO_3$, $CaSO_4{\cdot}2H_2O$ and $Al_2O_3{\cdot}xH_2O$ would coat the surface of the sample, thus occurring within the sampling depth of the Raman spectroscope. The calcium carbonate produced may be in the form of vaterite,[29] which has three characteristic ν_1 [CO_3^{2-}] bands at 1075 (strong), 1081 (weak) and 1090 cm^{-1} (very strong).[30] Moreover, the presence of gypsum would require an additional [SO_4^{2-}] band near 1010 cm^{-1}. Therefore, given that the ν_1 [SO_4^{2-}] band always appeared at 988 cm^{-1}, the direct carbonation of ettringite was disregarded in the current context. Finally, the carbonate anion can replace the sulfate anion in the ettringite structure, forming carbonate ettringite [$Ca_6Al_2(CO_3)_3(OH)_{12}{\cdot}26H_2O$][31] or thaumasite,[32] which can form solid solutions with ettringite. The carbonate and sulfate bands in thaumasite occur at 1072 and 990 cm^{-1}, respectively.[33] Clearly, the latter band could overlap with the 988 cm^{-1} band attributed to ettringite herein, but the absence of the 1072 cm^{-1} band, together with the ESEM results presented below, do not support the presence of thaumasite in the hydrated samples studied herein. This interpretation is further supported by the observation that the carbonate band at 1085 cm^{-1} increased in intensity relative to that of the ettringite band at 988 cm^{-1}, indicating that it reflected the growth of a separate species.

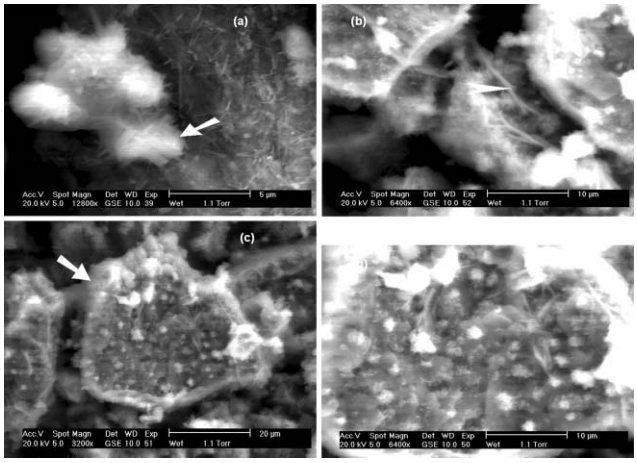

Fig. 7 ESEM images of Dycherhoff class G cement after 1 week's exposure to water vapour water.

Table 4 EDX elemental composition (mass%) of the features on cement

Element	Raw cement (average)	After 1 week		After 3 months	
		Fibre	Background	Fibre	Background
Al	1.6 ± 0.4	1.8	1.0	5.1	2.2
Ca	43.2 ± 2.0	15.8	24.8	43.4	20.8
S	1.6 ± 0.5	2.1	0.4	5.1	1.3
Si	11.8 ± 1.0	2.6	7.2	5.1	5.2
Mg	0.5 ± 0.2	0.2	0.5	0.4	0.2
Fe	2.2 ± 0.6	1.1	0.7	2.7	1.6
O	57.9 ± 1.0	76.1	65.0	36.7	68.0

2.2 ESEM. After 7 days' exposure to water vapour, phases of high aspect ratio began to develop in the cement powder and were visible using ESEM (Fig. 7), but not with the optical microscope, due to their small dimensions. Fibres were also observed in-between particles [Fig. 7(b), marked with an arrow]. The widespread presence of these fine whiskers [Fig. 7(a)] on particle surfaces suggested that the minerals adopting these structures were quite homogeneously dispersed in the cement. The elemental compositions of the high aspect ratio features, derived using EDX (Table 4), showed relatively higher contents of aluminium, calcium and sulfur compared with the average of those recorded on raw cement powders. In their study of *in situ* hydration of a cement, Stark *et al.*[21,22] suggested that the initial stage of hydration formed ettringite. It is unclear from the present EDX data whether these high aspect ratio features were indeed ettringite, but, given the high content of sulfur, aluminium and calcium, ettringite is certainly a strong candidate. Although the prominent feature in the morphology was the high aspect ratio particles, other significant features were present. Fig. 7(c) and (d) show that there were many small features created by etching/dissolution of cement particle surfaces, and the original particles appeared to be coated with a layer of amorphous material. EDX analysis suggested that the particle shown was alite. These observations, particularly the amorphous layer in the hydration of alite, are consistent with those made by Meredith *et al.*,[5] who assigned the amorphous coating to C–S–H gel.

Table 4 gives the elemental composition recorded on one of the fibrous features in Fig. 7. For comparison, the atomic ratios are presented in Table 5, along with those for pure ettringite and the average for the raw class G cement. The fibrous features had higher relative amounts of Ca, Al, Fe and S than the background, but were different to that of ettringite. The difference may arise from the small dimensions of the fibre, in that the EDX signal also contains information from the fibre

Table 5 Atomic ratios recorded at the points and comparison with theoretical data and average data for raw Dyckerdoff class G cement

Atomic ratio	Raw G (average)	After 1 week[a]		After 3 months[a]		Synthesised ettringite	Ettringite (theoretical)
		Fibre	Background	Fibre	Background		
Ca/Si	3.1	6.2	3.4	6.0	2.8		
Al/Ca	0.06	0.1	0.04	0.2	0.2	0.35	0.33
Fe/Ca	0.04	0.07	0.03	0.04	0.05		
S/Ca	0.01	0.13	0.017	0.13	0.08	0.5	0.5
Al/S	6	0.8	2.4	1.54	2.5	0.7	0.66

[a]Data derived assuming 24 oxygen atoms per molecules, as in ettringite ($Ca_6Al_2O_{12}$ $(SO_4)_3$, excluding oxygen atoms in H_2O molecules)

surroundings. Nevertheless, EDX data indicate that these high aspect ratio features did have higher contents of Al, Fe, S and Ca, which, together with the supporting XRD data, strongly suggests the presence of ettringite.

ESEM revealed that, after hydration for 3 months, the high aspect ratio features had grown in size, but were still fibrous. In addition, the surface of the cement sample was much flatter, with attendant growth of new features. These fibres exhibited a wide range of dimensions, with one measurement giving $\sim$1.2 microns in width and $>$10 microns in length [Fig. 8(A)]. There were also very fine whiskers associated with the initial stages of fibre growth around the cement particles, similar to those which had been observed after 1 week's exposure to water vapour.

An EDX spectrum recorded on one of the 3 month fibres [Fig. 8(B)] suggested the presence of Ca, S, Al and other elements. The EDX composition of the high aspect ratio structures produced after 3 months' exposure is compared with that after 1 week's exposure in Tables 4 and 5. Whilst the fibre had a similar Si content to the background, it clearly had a much higher content of aluminium, calcium and sulfur, and the concentration of these elements was higher than those recorded after 1 week's hydration. It should be noted that some of the X-rays may have originated from beneath the fibres, and the contribution from this would have a greater effect in the presence of the smaller fibres observed after 1 week's hydration. The atomic ratios for the fibres present after 1 week's exposure and after 3 months' exposure (Table 5), are very similar, suggesting that the two structures were essentially the same.

In order to confirm these features as ettringite, a synthetic ettringite was prepared following the procedure used by Hall.[34] X-Ray diffraction confirmed that it was ettringite with a small amount of gypsum, and ESEM showed that it had a fibrous structure. As anticipated, the composition of the synthesised ettringite agreed well with the theoretical values for ettringite ($Ca_6[Al_2(OH)_{12}].(SO_4)_3{\cdot}26H_2O$). Indeed the Al/S ratios (Table 5) determined for the fibrous whiskers after 1 week's exposure were almost identical to that for the synthetic ettringite and the theoretical ratio. Whilst this comparison does not unequivocally confirm that the fibrous structure was ettringite, it is likely that sulfur has been enriched at the underlying surface and, as shown above, the Raman microscopy was consistent with the material being ettringite. The fibres present after 3 months' exposure had a higher Al/S ratio than that for ettringite.

Since the band for carbonate at 1085 cm^{-1} was also present along with the sulfate band at 988 cm^{-1}, it was necessary to determine whether these bands were actually from the mineral thaumasite, $\{Ca_3[Si(OH)_6{\cdot}12H_2O](CO_3)(SO_4)\}$. EDX showed that there were significant amounts of both aluminium and silicon in the fibrous structure. However, elemental mapping of these features [Fig. 8(C)] revealed that the silicon distribution did not follow the star-like morphology, as aluminium did. With the lack of a band at 990 cm^{-1}, assigned to sulfate in thaumasite, as discussed previously,[33] it is suggested that these fibrous structures were due to ettringite with incorporated carbonate, possibly including in the form of carbonate ettringite. This is reasonable considering that it has been reported that thaumasite only forms at temperatures $\leqslant$5 °C, whereas these studies were performed at room temperature.[35,36]

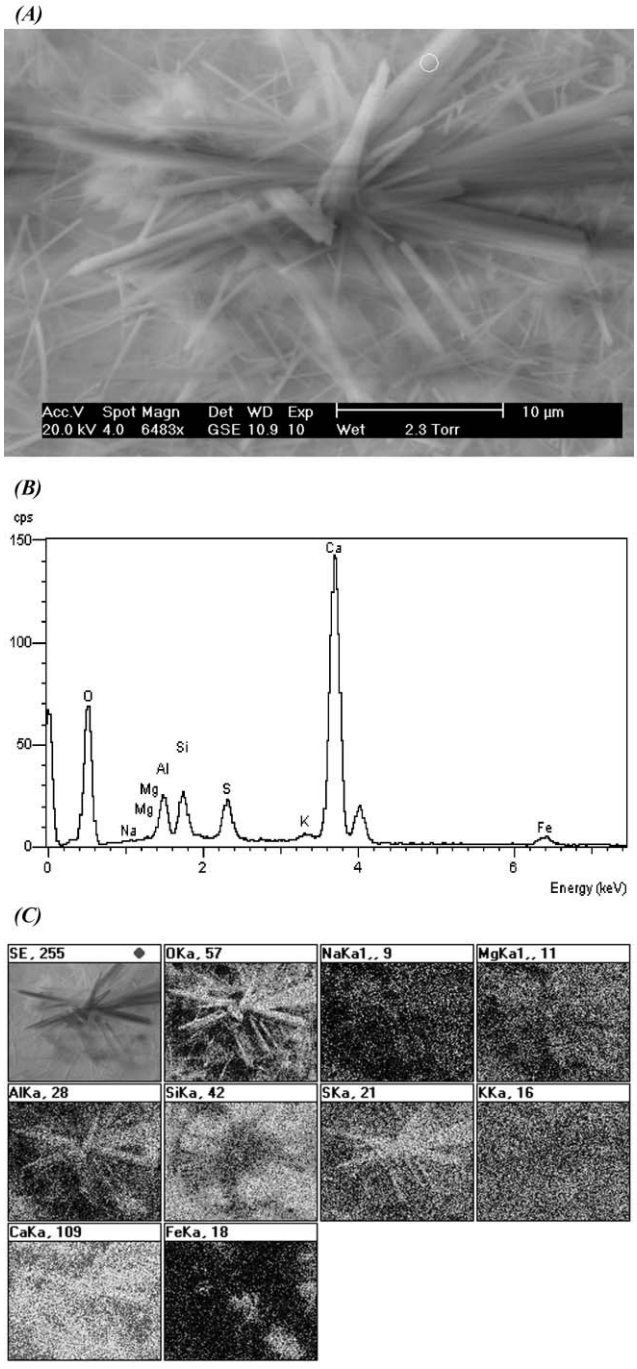

Fig. 8 (A) ESEM image of Dycherhoff class G cement after 3 months' exposure to water vapour water. (B) EDX spectrum recorded on one of the fibres (circled) in (A). (C) A series of elemental maps of the image in (A).

Summary and conclusions

Combined Raman microscopy and ESEM revealed the surface ageing processes of a Dyckerhoff class G cement that occurred when exposed to high humidity. The presence of carbon dioxide distinguishes the ageing process from the predominantly hydration processes of bulk cement. There is strong evidence that as sulfate dissolved into condensed surface water, C–S–H gel and ettringite formed, and that alite was preferentially hydrated. Carbon dioxide participated in the processes by forming calcium carbonate *via* reaction with calcium hydroxide. The study demonstrates the potential of combining the two techniques to obtain detailed, localised, *in situ* information on coupled chemical and structural changes in reactive mineral systems such as cements. The approach is being refined and developed for application to more detailed studies of cement particle hydration in cement pastes and slurries.

Acknowledgements

This project was financially supported by Schlumberger Cambridge Research (SCR). The ESEM-FEG was part funded by the European Regional Development Fund (EDRF) and the Raman microscope was funded by EPSRC. XRF data were provided by Margaret West and Bob Burton in the Materials Research Institute at Sheffield Hallam University. Helpful discussions with Professor Christopher Hall (University of Edinburgh) and Dr Louise Bailey (SCR) are gratefully acknowledged.

References

1 H. F. W. Taylor, *Cement Chemistry*, Thomas Telford, 2nd edn., 1997, ch. 7.
2 A. C. Jupe, X. Turrilas, P. Barnes, S. L. Colston, C. Hall, D. Häusermann and M. Hanfland, *Phys. Rev. B: Condens. Matter*, 1996, **53**, R14 97.
3 S. L. Colston, S. D. M. Jacques, P. Barnes, A. C. Jupe and C. Hall, *J. Synchrotron Radiat.*, 1998, **5**, 112–117.
4 P.-V. Vlachou and J. M. Piau, *Cem. Concr. Res.*, 1999, **29**, 27–36.
5 P. Meredith, A. M. Donald and K. Luke, *J. Mater. Sci.*, 1995, **30**, 1921–1930.
6 E. Breval, *Cem. Concr. Res.*, 1977, **7**, 297.
7 O. M. Jensen, P. F. Hansen, E. E. Lachowski and F. P. Glasser, *Cem. Concr. Res.*, 1999, **29**, 1505.
8 K. Thiesen and V. Johansen, *Am. Ceram. Soc. Bull.*, 1975, **54**, 787.
9 T. C. Powers, *Proc. Natl. Highways Res. Board*, 1947, **27**, 178.
10 P. Fletcher and P. Coveney, *Adv. Cem. Based Mater.*, 1995, **2**, 21–29.
11 T. L. Hughes, C. M. Methven, T. G. J. Jones, S. E. Pelham and P. Franklin, in *Recent Advances in Oilfield Chemistry*, ed. P. H. Ogden, The Royal Society of Chemistry, Cambridge, 1994, pp. 99–115.
12 J. Bensted, *J. Am. Ceram. Soc.*, 1976, **59**, 140–143.
13 J. Bensted, *Cem. Concr. Res.*, 1977, **7**, 161–164.
14 R. G. Herman, C. B. Bogdan, A. J. Sommer and D. R. Simpson, *Appl. Spectrosc.*, 1987, **41**, 437.
15 C. D. Dyer, P. Hendra and W. Forsling, *Spectrochim. Acta, Part A*, 1993, **49**, 715–722.
16 M. Tarrida, M. Madon, B. Le Rolland and P. Colombet, *Adv. Cem. Based Mater.*, 1995, **2**, 15–20.
17 R. J. Kirkpatrick, J. L. Yarger, P. F. McMillan, P. Yu and X. Cong, *Adv. Cem. Based Mater.*, 1997, **5**, 93–99.
18 X.-D. Cong and R. J. Kirkpatrick, *Adv. Cem. Based Mater.*, 1996, **3**, 144–156.
19 See, for example: H. R. Steward and J. E. Bailey, *J. Mater. Sci.*, 1983, **18**, 3686.
20 See, for example: S. Chatterji and J. W. Jeffery, *Nature*, 1966, **209**, 1223.
21 J. Stark, B. Moser and A. Eckart, *ZKG Int.*, 2001, **54**, 52–60.
22 J. Stark, B. Moser and A. Eckart, *ZKG Int.*, 2001, **54**, 114–119.
23 R. H. Bogue, *Ind. Eng. Chem. Anal.*, 1929, **1**, 192 , but modified as detailed in ref. 1, p. 57.
24 M. Conjeau and H. Boyer, *Cem. Concr. Res.*, 1980, **10**, 61–70.
25 M. Hanke, *Appl. Spectrosc.*, 1986, **40**, 871–877.
26 C. Remy, B. Reynard and M. Madon, *J. Am. Ceram. Soc.*, 1997, **80**(2), 413–23.
27 K. Fukuda, A. Takeda, A. Yamaguchi and S. Hashimoto, *J. Am. Ceram. Soc.*, 2001, **84**(5), 1155–60.
28 C. Hall and K. L. Scrivener, *Adv. Cem. Based Mater.*, 1998, **7**, 28–38.
29 Q. Zhou and F. P. Glasser, *Adv. Cem. Res.*, 2000, **12**(3), 131–136.
30 R. W. Gauldie, S. K. Sharma and E. Volk, *Comp. Biochem. Physiol., A: Physiol.*, 1997, **118**(3), 753–757.
31 S. J. Barnet, C. D. Adam and A. R. W. Jackson, *Cem. Concr. Res.*, 2001, **31**, 13.
32 S. J. Barnet, C. D. Adam and A. R. W. Jackson, *J. Mater. Sci.*, 2000, **35**, 4109.
33 A. R. Brough and A. Atkinson, *Cem. Concr. Res.*, 2001, **31**, 421–424.
34 C. Hall, P. Barnes, A. D. Billimore, A. C. Jupe and X. Turrilas, *J. Chem. Soc., Faraday Trans.*, 1996, **92**(12), 2125–2129.
35 J. Bensted, *Cem. Concr. Res.*, 1999, **21**, 117–121.
36 J. Aguilera, M. T. B. Varela and T. Vazquez, *Cem. Concr. Res.*, 2001, **31**, 1163–1168.